

Multifractal behaviour in multiparticle production in pp collisions at $\sqrt{s} = 0.9, 7$ and 8 TeV from the CMS experiment

Z. Ong, P. Agarwal, H.W. Ang, A.H. Chan, C.H. Oh

Department of Physics, National University of Singapore

Abstract

Multifractal analysis was performed on pp collision data at $\sqrt{s} = 0.9, 7$ and 8 TeV from the CMS experiment at CERN. The data was obtained and processed from the CERN Open Data Portal. Vertical analysis was used to compute the generalised dimensions D_q and the multifractal spectra $f(\alpha)$ of the data, which reveals the level of complexity of its pseudorapidity distribution. It was found that the $f(\alpha)$ curves widen with increasing collision energy, signalling an increase in branching complexity.

1 Multifractal formalism for multiparticle production

Multifractal analysis is a powerful tool used to characterise the complexity of data. It is highly multidisciplinary in nature, finding applications in the analysis of a wide variety of complex systems, such as studying tectonic processes [1], medical signal analysis [2] and time series analysis in meteorology [3]. Here, we re-introduce a formalism tailored for investigating multiparticle production, as formulated by Hwa [4]. As with the original formulations, rapidity y will be used in the presentation, but will be substituted with pseudorapidity η when processing the data.

G-moments

Multifractal analysis in the context of multiparticle production was originally done by computing the G -moments of multiplicity distributions [4–6]. We begin by considering a single rapidity interval δy and a collection of N events. Each event i has multiplicity n_i , and $K = \sum_{i=1}^N n_i$ is the total number of particles in δy summed over all events.

The G -moment for the collection of N events in δy is then defined as

$$G_q(\delta y) = \sum_{i=1}^N p_i^q, \quad (1)$$

where $p_i = \frac{n_i}{K}$ is the probability of finding a particle in the i^{th} event. The prime indicates G_q is summed only over non-empty events (i.e. all $p_i > 0$), so we can have $q \in \mathbb{R}$. However, $G_q(\delta y)$ is very sensitive to statistical fluctuations for small N , and modified definitions have been proposed in [7].

The quantity being summed over (p_i in our case) is called a *measure*. q acts as a probing parameter – higher values would enhance the differences between the p_i 's. Changing δy explores the phase space at different scales. As such, $G_q(\delta y)$ is sometimes called the partition function in multifractal analysis [1] as it encodes information at different scales δy and at different moments q . This scheme of setting up $G_q(\delta y)$ is analogous to the box counting algorithm commonly used in digital image analysis.

Properties of $G_q(\delta y)$

Suppose that for some event i , its p_i value scales as

$$p_i \propto (\delta y)^{\alpha_i} \quad (2)$$

for some exponent α_i . For a multifractal system, the α_i 's are generally different and can take on a range of values, reflecting different subsets of the data with local scaling behaviour¹. Let $S_{\alpha'}$ be a set

¹If all α_i 's are equal, the system is a monofractal.

containing all the events that scale according to equation 2, with the same value of α' . Furthermore, let $N_{\alpha'}(\delta y)$ denote the cardinality of $S_{\alpha'}$. Multifractals generally have the property that [1, 4]

$$N_{\alpha'}(\delta y) \propto (\delta y)^{-f(\alpha')}, \quad (3)$$

i.e. the collection of events that scale according to equation 2 with a particular value of α' in a particular window $[\alpha', \alpha' + d\alpha']$ form a fractal subset (of a larger set of more fractal subsets corresponding to other values of α), and its cardinality scales with fractal dimension $f(\alpha')$. It is in this sense that the union of fractal subsets form a multifractal.

$N_{\alpha'}(\delta y)$ has been suggested by Halsey *et al.* [8] to be of the form [4]

$$N_{\alpha'}(\delta y) = \int_{\alpha'}^{\alpha' + d\alpha'} d\alpha h(\alpha) (\delta y)^{-f(\alpha)}, \quad (4)$$

for some continuous function $h(\alpha)$. With equation 4, we can now re-express $G_q(\delta y)$ as

$$\begin{aligned} G_q(\delta y) &= \sum_{m=1}^M p_m^q \\ &\propto \sum_{m=1}^M (\delta y)^{q\alpha_m} \\ &= \int d\alpha h(\alpha) (\delta y)^{-f(\alpha)} (\delta y)^{q\alpha} \\ &= \int d\alpha h(\alpha) (\delta y)^{q\alpha - f(\alpha)}. \end{aligned} \quad (5)$$

The resulting dependence of $G_q(\delta y)$ on δy can be expressed as [4]

$$G_q(\delta y) \propto (\delta y)^{\tau(q)}, \quad (6)$$

where $\tau(q)$ has been established by Hentschel and Procaccia [9] to be

$$\tau(q) = (q - 1)D_q. \quad (7)$$

D_q is known as the generalised dimension of order q , which can be experimentally obtained by rearranging equation 7:

$$D_q = \lim_{\delta y \rightarrow 0} \left[\frac{1}{q - 1} \frac{\ln G_q(\delta y)}{\ln(\delta y)} \right]. \quad (8)$$

It must be noted that in experimental measurements, the mathematical limit $\delta y \rightarrow 0$ in equation 8 cannot be realised. The finiteness of particle multiplicity produced from finite energy implies that self-similar and fractal structures, if present, cannot persist indefinitely to finer scales of resolution [10]. Additionally, the detector resolution also imposes a lower limit on the probing scale.

The goal in multifractal analysis is to study the dependence of $G_q(\delta y)$ on δy , and the D_q 's are the main quantities that summarise the relation. D_0 , D_1 and D_2 are also known as the *fractal*, *information*² and *correlation* dimensions respectively [4, 9]. A monofractal has constant D_q for all q ; otherwise, it is a multifractal [1].

The above approach using the G -moments does not assume any specific dynamical model of multi-particle production [10], which serves as a model-agnostic tool to describe the complexity within data.

2 Vertical and horizontal averaging

By construction, the G -moment described in the previous section accesses a very small subset of the data – only one rapidity interval over all N events. The G -moments computed this way is also known as the vertical moments [4], notated as $G_q^{(v)}$.

Alternatively, one can also analyse all the rapidity intervals in a single event. The G -moments computed this way is known as the horizontal moments [4], notated as $G_q^{(h)}$.

²For $q = 1$, the singularity in $1/(q - 1)$ is handled by taking the limiting value as $q \rightarrow 1$.

Since both methods access only a small slice of the available data, the statistics can be enhanced by supplementing the vertical moments with horizontal averaging, and vice versa. For example, the vertical moments can be calculated for every δy interval and averaged horizontally over the M bins:

$$\langle G_q^{(v)} \rangle \equiv \frac{1}{M} \sum_m^M G_q^{(v)}. \quad (9)$$

Likewise, the horizontal moments can be calculated for every event and averaged vertically over all N events:

$$\langle G_q^{(h)} \rangle \equiv \frac{1}{N} \sum_i^N G_q^{(h)}. \quad (10)$$

In general, we have $\langle G_q^{(v)} \rangle \neq \langle G_q^{(h)} \rangle$ except when $q = 1$. The two moments also capture different features of the dataset; for example, $\langle G_q^{(v)} \rangle$ would be sensitive to rare events with very high multiplicity, while $\langle G_q^{(h)} \rangle$ would not. $\langle G_q^{(h)} \rangle$ however, describes a more intuitive notion of fractal structures within the multiparticle production in each event. Florkowski and Hwa [10] have studied the limiting scenarios in which they are equivalent, under the assumptions of ergodicity.

Contemporary multiplicity measurements (e.g. [11]) are statistically derived quantities, with $P(n)$ interpreted as an average over many events that has undergone an unfolding process. The pseudorapidity distribution of single events is not available as a result. Hence, we will perform our multifractal analysis using the vertical moments with horizontal averaging (equation 9).

3 The $f(\alpha)$ spectrum

As multifractals cannot be described by a single fractal dimension, a *singularity spectrum* or *Legendre spectrum*, $f(\alpha)$ is used to characterise them instead, which encodes the spread of α values exhibited by the system.

To obtain the $f(\alpha)$ spectrum, consider again equation 5:

$$G_q(\delta y) = \int d\alpha h(\alpha) (\delta y)^{q\alpha - f(\alpha)}.$$

Suppose $h(\alpha) \neq 0$. For each value of q and in the limit $\delta y \rightarrow 0$, the integral would have most of its contribution from some value α which makes the exponent $q\alpha - f(\alpha)$ smallest. Let this optimising value of α be α_q . To minimise the exponent, we require

$$\left. \frac{d}{d\alpha} [q\alpha - f(\alpha)] \right|_{\alpha=\alpha_q} = 0, \quad (11)$$

$$\left. \frac{d^2}{d\alpha^2} [q\alpha - f(\alpha)] \right|_{\alpha=\alpha_q} > 0, \quad (12)$$

which result in

$$f'(\alpha_q) = q, \quad (13)$$

$$f''(\alpha_q) < 0. \quad (14)$$

Substituting equations 13 and 14 into 8, and using the saddle point approximation, we get

$$\begin{aligned} D_q &= \lim_{\delta y \rightarrow 0} \left[\frac{1}{q-1} \frac{\ln G_q(\delta y)}{\ln(\delta y)} \right] \\ &= \lim_{\delta y \rightarrow 0} \left[\frac{1}{q-1} \frac{\ln \int d\alpha h(\alpha) (\delta y)^{q\alpha - f(\alpha)}}{\ln(\delta y)} \right] \\ &\approx \lim_{\delta y \rightarrow 0} \left[\frac{1}{q-1} \frac{\ln [d\alpha h(\alpha_q) (\delta y)^{q\alpha_q - f(\alpha_q)}]}{\ln(\delta y)} \right] \\ &= \lim_{\delta y \rightarrow 0} \left[\frac{1}{q-1} \frac{\ln [d\alpha h(\alpha_q)] + \ln(\delta y)^{q\alpha_q - f(\alpha_q)}}{\ln(\delta y)} \right] \\ \therefore D_q &\approx \frac{q\alpha_q - f(\alpha_q)}{q-1} = \frac{\tau(q)}{q-1}. \end{aligned} \quad (15)$$

Equation 15 reveals how all the quantities in multifractal analysis relate to each other and how they can be computed. First, $\tau(q)$ can be evaluated by [4]

$$\tau(q) = \lim_{\delta y \rightarrow 0} \left[\frac{\ln G_q(\delta y)}{\ln(\delta y)} \right], \quad (16)$$

which also gives D_q via equation 8. In our analysis, $G_q(\delta y)$ will be replaced by $\langle G_q^{(v)} \rangle$ (equation 9).

Next, α_q is obtained via numerical differentiation [4]:

$$\alpha_q = \frac{d}{dq} \tau(q). \quad (17)$$

This finally allows us to compute $f(\alpha)$ [4]:

$$f(\alpha_q) = q\alpha_q - \tau(q). \quad (18)$$

For a multifractal, equations 13 and 14 indicate that the curve $f(\alpha)$ has a maximum at α_0 and is concave downward everywhere. In the case of a monofractal, only a single value of α exists and the $f(\alpha)$ spectrum would reduce to a point [1].

What does the $f(\alpha)$ curve tell us?

In general, $f(\alpha)$ curves in multifractal analysis describes the *complexity* of a signal [1]. In the context of our analysis, it describes the smoothness (or roughness) of the pseudorapidity distribution of our multiplicity data, $N(\eta)$. A low value of α_0 indicates a smoother $N(\eta)$. The width W reflects the range of fractal exponents embedded in the dataset – larger values of W reflect a more complex $N(\eta)$ distribution (i.e. greater degree of multifractality).

4 About the data

This analysis is performed on Run 1 data from the CMS collaboration processed from the CMS Open Data Portal, covering centre-of-mass energies $\sqrt{s} = 0.9, 7$ and 8 TeV. The analysis method follows largely that of CMS [11], which analysed minimum-bias (MinBias), non-single diffractive (NSD) multiplicity distributions.

NSD events were selected by requiring that at least one forward hadron (HF) calorimeter tower on each side of the detector have at least 3 GeV of energy deposited in the event. The primary vertex was chosen as the vertex with the highest number of associated tracks, which must also be within 15 cm of the reconstructed beamspot in the beam axis and be of good reconstruction quality ($\text{ndof} > 4$).

Good quality tracks were selected by requiring them to carry the `highPurity` label. Furthermore, we select for tracks with $<10\%$ relative error on the transverse momentum (p_T) measurement ($\sigma_{p_T}/p_T < 0.1$) to reject low-quality and badly reconstructed tracks. Secondaries were removed by requiring a small impact parameter with respect to the selected primary vertex. Also, tracks were required to have $p_T > 500$ MeV/c, which will be extrapolated to zero via unfolding.

Finally, unfolding was performed using an iterative ‘‘Bayesian unfolding method’’, which is more accurately known as ‘‘D’Agostini iteration with early stopping’’ and described in [12]. This infers the original charged hadron multiplicity distribution (MinBias NSD) from the charged track multiplicity distribution measured.

Tables 2 and 3 in the Appendix summarise the datasets used.

5 Results and Discussion

Table 1 summarises the results of our multifractal analysis, giving the generalised dimensions D_q and an approximate description of the width of the $f(\alpha)$ curves.

Mathematically, the data points that constitute the $f(\alpha)$ curves are plotted by evaluating equation 18 for $q \in \mathbb{R}$. However, this is computationally impossible, as equation 1 would produce infinities for $q \rightarrow -\infty$ and infinitesimally small values for $q \rightarrow +\infty$; both scenarios would lead to numerical instabilities. Since the goal is to obtain a relative comparison of the widths of the $f(\alpha)$ curves, we restricted the

Table 1: Generalised dimensions and width of $f(\alpha)$ curves from multifractal analysis of pp collisions at $\sqrt{s} = 0.9, 7$ and 8 TeV, with all values normalised to D_0 at $\sqrt{s} = 900$ GeV. α_{\max} and α_{\min} are evaluated at $q = -20$ and $q = +20$ respectively.

\sqrt{s}	900 GeV	7 TeV	8 TeV
D_0	1	0.996	0.996
D_1	0.988	0.980	0.978
D_2	0.975	0.965	0.961
D_3	0.964	0.952	0.948
D_4	0.954	0.941	0.937
D_5	0.946	0.932	0.927
α_{\min}	0.838	0.829	0.826
α_{\max}	1.054	1.068	1.072
W	0.216	0.239	0.246

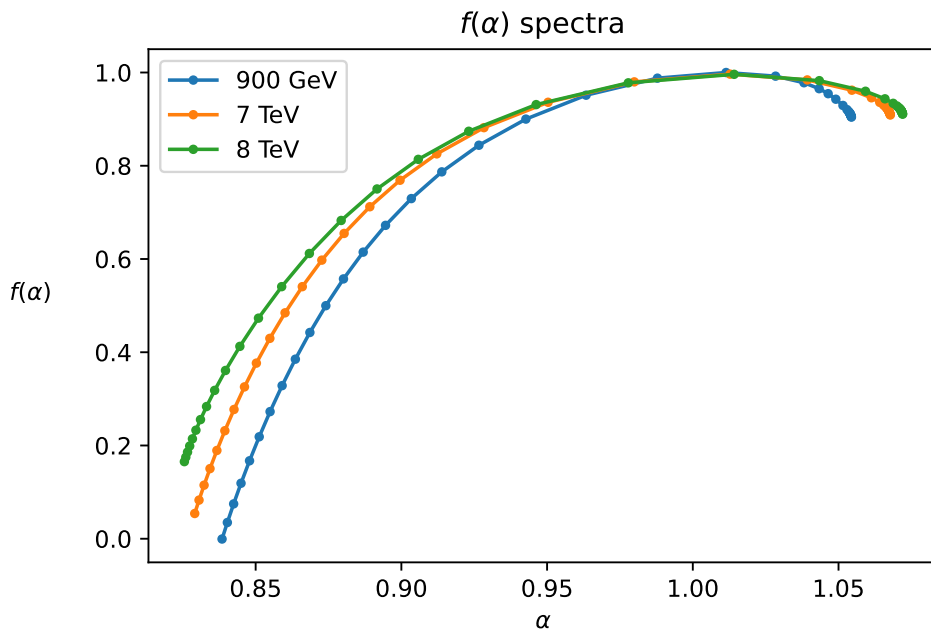


Figure 1: $f(\alpha)$ spectra of pp collisions at $\sqrt{s} = 0.9, 7$ and 8 TeV.

computation of data points to $-20 \leq q \leq 20$. The distance between these data points at these limiting values of q in the α -axis would be our estimate³ of the $f(\alpha)$ width, W .

Figure 1 shows that the $f(\alpha)$ curves clearly broaden with increasing collision energy (which is also detailed in Table 1). This is a reflection of increasing complexity in the multiplicity data.

6 Conclusion

The techniques in multifractal analysis provide a model-independent means of describing the inherent complexity within the structures of the multiplicity distribution. We have used it to analyse pp collisions at $\sqrt{s} = 0.9, 7$ and 8 TeV and found that the $f(\alpha)$ curves broaden with increasing collision energy. This reflects an increase in complexity of the pseudorapidity distribution of the data. At higher energies, we would expect the $f(\alpha)$ curves to broaden further.

³Some studies (e.g. [1]) estimate W by performing a simple fit of $f(\alpha)$ to a quadratic function and taking the distance between the roots. However, this assumes that $f(\alpha)$ is inherently quadratic, which is not always true.

A Datasets used

Table 2: Summary of CMS collider datasets used from CERN Open Data Portal

\sqrt{s} (TeV)	Dataset	Ref.
0.9	/MinimumBias/Commissioning10-07JunReReco_900GeV/RECO	[13]
7	/MinimumBias/Run2010A-Apr21ReReco-v1/AOD	[14]
8	/MinimumBias/Run2012B-22Jan2013-v1/AOD	[15]

Table 3: Summary of Monte Carlo datasets used from CERN Open Data Portal

\sqrt{s} (TeV)	Dataset	Ref.
0.9	/MinBias_TuneZ2_900GeV_pythia6.cff_py _GEN_SIM_START311_V2_Dec11_v2	[16]
7	/MinBias_TuneZ2star_7TeV_pythia6/Summer12-LowPU2010 _DR42-PU_S0_START42_V17B-v1/AODSIM	[17]
8	/MinBias_TuneZ2star_8TeV-pythia6/Summer12_DR53X-PU _S10_START53_V7A-v1/AODSIM	[18]

References

- ¹L. Telesca, G. Colangelo, V. Lapenna, and M. Macchiato, “Monofractal and multifractal characterization of geoelectrical signals measured in southern italy”, *Chaos, Solitons & Fractals* **18**, 385–399 (2003).
- ²R. Lopes and N. Betrouni, “Fractal and multifractal analysis: a review”, en, *Medical Image Analysis* **13**, 634–649 (2009).
- ³J. Krzyszczak, P. Baranowski, M. Zubik, V. Kazandjiev, V. Georgieva, C. Sławiński, K. Siwek, K. Jerzy, and A. Nieróbca, “Multifractal characterization and comparison of meteorological time series from two climatic zones”, *Theoretical and Applied Climatology* **137**, 10.1007/s00704-018-2705-0 (2019).
- ⁴R. C. Hwa, “Fractal Measures in Multiparticle Production”, *Phys. Rev. D* **41**, 1456 (1990).
- ⁵L. K. Chen, A. H. Chan, and C. K. Chew, “Multifractality and high-energy multiparticle production”, *Z. Phys. C* **60**, 503–507 (1993).
- ⁶E. A. De Wolf, I. M. Dremin, and W. Kittel, “Scaling laws for density correlations and fluctuations in multiparticle dynamics”, *Phys. Rept.* **270**, 1–141 (1996).
- ⁷R. C. Hwa and J.-c. Pan, “Fractal behavior of multiplicity fluctuations in high-energy collisions”, *Phys. Rev. D* **45**, 1476–1483 (1992).
- ⁸T. C. Halsey, M. H. Jensen, L. P. Kadanoff, I. Procaccia, and B. I. Shraiman, “Fractal measures and their singularities: The characterization of strange sets”, *Phys. Rev. A* **33**, [Erratum: *Phys.Rev.A* 34, 1601 (1986)], 1141–1151 (1986).
- ⁹H. G. E. Hentschel and I. Procaccia, “The infinite number of generalized dimensions of fractals and strange attractors”, *Physica* **8**, 435–444 (1983).
- ¹⁰W. Florkowski and R. C. Hwa, “Universal multifractality in multiparticle production”, *Phys. Rev. D* **43**, 1548–1554 (1991).
- ¹¹V. Khachatryan et al., “Charged Particle Multiplicities in pp Interactions at $\sqrt{s} = 0.9, 2.36, \text{ and } 7$ TeV”, *JHEP* **01**, 079 (2011).
- ¹²G. D’Agostini, “A Multidimensional unfolding method based on Bayes’ theorem”, *Nucl. Instrum. Meth. A* **362**, 487–498 (1995).

- ¹³CMS collaboration (2019), “MinimumBias primary dataset in RECO format from the 0.9 TeV Commissioning run of 2010 (/MinimumBias/Commissioning10-07JunReReco_900GeV/RECO). CERN Open Data Portal.
DOI:10.7483/OPENDATA.CMS.1R58.OMBD”,
- ¹⁴CMS collaboration (2019), “MinimumBias primary dataset in AOD format from RunA of 2010 (/MinimumBias/Run2010A-Apr21ReReco-v1/AOD). CERN Open Data Portal.
DOI:10.7483/OPENDATA.CMS.6B3H.TR6Z”,
- ¹⁵CMS collaboration (2017), “MinimumBias primary dataset in AOD format from RunB of 2012 (/MinimumBias/Run2012B-22Jan2013-v1/AOD). CERN Open Data Portal.
DOI:10.7483/OPENDATA.CMS.HU6U.DRLD”,
- ¹⁶CMS Collaboration (2019), “Simulated dataset MinBias_TuneZ2_900GeV_pythia6_cff_py_GEN_SIM_START311_V2_Dec11_v2 in GEN-SIM-RECO format for 2010 commissioning data. CERN Open Data Portal.
DOI:10.7483/OPENDATA.CMS.JPB5.X7CN”,
- ¹⁷CMS Collaboration (2018), “Simulated dataset MinBias_TuneZ2star_7TeV_pythia6 in AODSIM format for 2010 collision data. CERN Open Data Portal.
DOI:10.7483/OPENDATA.CMS.VTJ2.E5JN”,
- ¹⁸CMS Collaboration (2021), “Simulated dataset MinBias_TuneZ2star_8TeV_pythia6 in AODSIM format for 2012 collision data. CERN Open Data Portal.
DOI:10.7483/OPENDATA.3GIM.7SPW”,